Analytica Chimica Acta 737 (2012) 22–28

Contents lists available at SciVerse ScienceDirect

Analytica Chimica Acta

journal homepage: www.elsevier.com/locate/aca

Magnetic Fe_3O_4@Au composite-enhanced surface plasmon resonance for ultrasensitive detection of magnetic nanoparticle-enriched α-fetoprotein

Ru-Ping Liang, Gui-Hong Yao, Li-Xia Fan, Jian-Ding Qiu*

Department of Chemistry and Institute for Advanced Study, Nanchang University, Nanchang 330031, China

HIGHLIGHTS

- We report an amplification technique using Fe_3O_4@Au MNPs for an SPR bioassay.
- Fe_3O_4@Au MNPs can function as an amplifier to increase the SPR signal.
- Sensitive detection of AFP is achieved via the purification/amplification protocol.
- This strategy has great potential for detecting other biomolecules of interest.

GRAPHICAL ABSTRACT

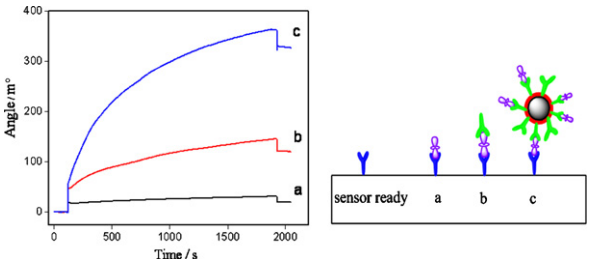

ARTICLE INFO

Article history:
Received 30 March 2012
Received in revised form 8 May 2012
Accepted 14 May 2012
Available online 9 June 2012

Keywords:
Surface plasmon resonance
Fe_3O_4@Au magnetic nanoparticle
α-Fetoprotein
signal enhancement

ABSTRACT

Small molecules or analytes present at low concentrations are difficult to detect directly using conventional surface plasmon resonance (SPR) techniques because only small changes in the refractive index of the medium are typically induced by the binding of these analytes. Here, we present an amplification technique using core–shell Fe_3O_4@Au magnetic nanoparticles (MNPs) for an SPR bioassay. To evaluate this amplification effect, a novel SPR sensor based on a sandwich immunoassay was developed to detect α-fetoprotein (AFP) by immobilizing a primary AFP antibody (Ab_1) on the surface of a 3-mercapto-1-propanesulfonate/chitosan-ferrocene/Au NP (MPS/CS-Fc/Au NP) film employing Fe_3O_4@Au–AFP secondary antibody conjugates (Fe_3O_4@Au–Ab_2) as the amplification reagent. The stepwise fabrication of the biosensor was characterized using UV-vis spectroscopy, electrochemical impedance spectroscopy, and cyclic voltammetry. A calibration curve of Fe_3O_4@Au–Ab_2 conjugates amplification for AFP detection was obtained to yield a correlation in the range of 1.0–200.0 ng mL^{-1} with a detection limit of 0.65 ng mL^{-1}, and a significant increase in sensitivity was therefore afforded through the use of Fe_3O_4@Au–Ab_2 conjugates as an amplifier. This magnetic separation and amplification strategy has great potential for the detection of other biomolecules of interest with low interference and high sensitivity by changing the antibody label used in the Fe_3O_4@Au–antibody conjugates.

1. Introduction

Surface plasmon resonance (SPR) is an optical physical phenomenon produced by the optical coupling of thin metal films. Since the first application of SPR technology for a biosensor in 1983 [1], SPR biosensors have attracted increasing attention and have been widely used in various fields including medical diagnostics [2], environmental monitoring [3], food safety [4,5], and security [6]. SPR biosensors have become powerful tools, offering real-time monitoring, label-free detection, and high-specificity binding for characterizing and quantifying biomolecular interactions. However, one of the main drawbacks of SPR biosensors is that the SPR system has insufficient sensitivity to detect small molecules or low-concentration compounds at the sensing surface because

* Corresponding author. Tel.: +86 791 83969518.
E-mail addresses: jdqiu@ncu.edu.cn, qiujianding@163.com (J.-D. Qiu).

0003-2670/$ – see front matter © 2012 Elsevier B.V. All rights reserved.
http://dx.doi.org/10.1016/j.aca.2012.05.043

the binding of such analytes causes only a small change in the refractive index of the medium [7]. With the recent development of the life sciences, the requirement of high-sensitivity technologies for the detection and quantification of biological samples with low molecular weights and/or at low concentrations has become increasingly important [8]. Therefore, the development of sensitivity enhancements for SPR biosensors is urgently required to extend the range of application of these tools.

Several approaches have been attempted to enhance SPR detection sensitivity including the use of a resonant mirror [9], a grating coupler [10], signal-to-noise optimization [11], and adopting a sandwich detection format with a second antibody as an amplifier, which is similar to the enzyme-linked immunosorbent assay method [12]. However, these methods suffer from narrow linear ranges and limited signal enhancement and thus cannot enable ultrasensitive detection [13]. Because the surface plasmon used in SPR spectroscopy is highly sensitive to changes in the refractive index of the material near the sensor surface due to binding events, especially for molecules with high masses, various metal nanoparticles including Ag NPs [8], Pd NPs [14], Au NPs [7,15–18], and Pt NPs [19] have been used extensively in efforts to enhance the sensitivity of the SPR response due to their high molecular weights and the coupling of the localized surface plasmon of metal nanoparticles with the propagating plasmon on the SPR gold surface [7]. For example, Lyon et al. [20] described an immunosensor for the detection of h-IgG using colloidal Au as a label to obtain a 25-fold larger signal than that observed in the absence of the Au particle. Although these methods allow for sensitivity enhancements, a shortcoming of a time-consuming and complex process is generally required when applied in the selective enrichment and separation of target molecules from a sample solution as centrifugation, especially when detecting analytes present in complex samples.

More recently, magnetic nanoparticles (MNPs) have received increasing attention due to their high surface-to-volume ratios, allowing for a high density of chemical binding, their excellent magnetic properties, allowing for the direct capture and easy separation and concentration of targets in complex samples in an external magnetic field, and their high refractive indices and high molecular weights, which can effectively increase an SPR signal [21]. These advantages make MNPs desirable candidates for SPR bioassays, as they can function as both an amplifier to increase the sensitivity of the SPR biosensor and simultaneously as a concentration/purification agent to reduce background interference. Although MNPs are excellent agents for a low-interference and sensitive SPR biosensor, they suffer from several drawbacks such as a lack of surface tunability for biocompatible applications [22], which makes them difficult to couple with biomolecules directly. Additionally, MNPs readily aggregate and lose their magnetic properties when applied in complex environmental and biological systems [23]. To address these problems, magnetic core–shell nanoparticles that have Fe_3O_4 cores with shells consisting of a metal or a metal oxide such as gold [24,25], silver [26], silica [27,28], titania [29], or alumina [30] have been extensively tested. Au has been reported to be one of the best candidate shell materials for the fabrication of novel magnetic core–shell NPs, exhibiting the desirable intrinsic properties of the magnetic core and an Au shell. However, the majority of prior studies have focused on employing Fe_3O_4@Au MNPs as special biomolecule-immobilizing carriers for bioseparations, and only a limited number of studies have investigated the amplification effect of Fe_3O_4@Au MNPs or the use of Fe_3O_4@Au MNPs as labels to enhance biodetection in SPR-based bioassays.

Here, we report a protocol for the elaboration of a core–shell Fe_3O_4@Au MNP-based amplification strategy for the low-interference, high-sensitivity SPR detection of the model protein α-fetoprotein (AFP), a tumor marker that is widely used for the diagnosis of hepatocellular carcinoma [31]. The Fe_3O_4@Au MNPs not only have magnetic Fe_3O_4 cores that allow for their easy manipulation in an external magnetic field but also have excellent biocompatibility; the ability to add surface functionality to the Au layer provides an interface for the assembly of antibody molecules while maintaining their bioactivity, which can be investigated using UV-vis spectroscopy. A sandwich-type protocol was successfully introduced to develop an SPR immunoassay by immobilizing the primary antibody on the surface of an MPS/CS-Fc/Au NP film and then capturing the AFP antigen molecules, which are reacted with a secondary antibody labeled with Fe_3O_4@Au MNPs (Scheme 1). Due to the high refractive index and high molecular weight of the Fe_3O_4@Au MNPs and the electronic coupling interaction between the Au shell and the surface plasmon wave associated with the SPR gold film, Fe_3O_4@Au MNPs significantly amplify the SPR signal; moreover, the adsorbed colloidal Au onto the self-assembled monolayer (SAM) formed on the SPR substrate could collectively or selectively alter the three signature SPR features of the substrate/SAM system, thereby enhancing the detection sensitivity of the SPR device [32]; thus, sensitive detection of the AFP antigen is achieved via this simple purification/concentration/amplification procedure. The proposed amplified detection strategy can be used to detect other biomolecules of interest by changing the corresponding antibody in the Fe_3O_4@Au–antibody conjugates.

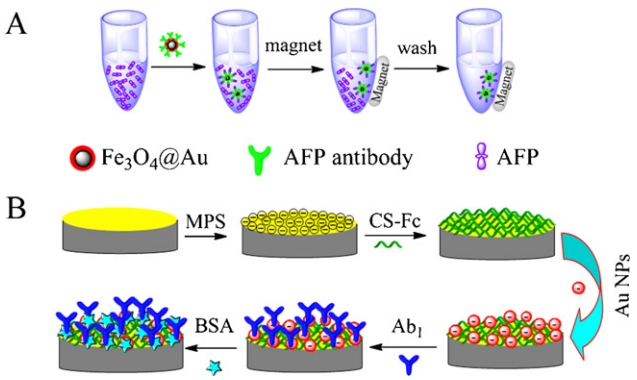

Scheme 1. The steps for processing samples with Fe_3O_4@Au–Ab_2 MNPs (A). A schematic illustration of the stepwise preparation process of the sensor surface (B).

2. Materials and methods

2.1. Reagents

Polyclonal mouse anti-human α-fetoprotein antibody (Ab_1), α-fetoprotein antibody (Ab_2), and AFP were purchased from Bio-Cell Co., Ltd. (Zhengzhou, China). Hydrogen tetrachloroaurate ($HAuCl_4{\cdot}4H_2O$), (3-aminopropyl)triethoxysilane (APTES), bovine serum albumin (BSA), chitosan (CS, 85% deacetylation), ferrocenecarboxaldehyde (FcCHO, 98%), and sodium 3-mercapto-1-propanesulfonate (MPS) were purchased from Sigma (St. Louis, USA). Phosphate-buffered saline (PBS) was prepared by varying the ratio of 0.1 M Na_2HPO_4 and 0.1 M KH_2PO_4. All other chemicals were of analytical grade and used as received without further purification. All aqueous solutions were prepared with double-distilled water.

2.2. Apparatus

The UV–vis absorption spectra of Fe_3O_4, Fe_3O_4@Au, and Fe_3O_4@Au–Ab_2 were obtained with an UV-2450 ultraviolet-visible spectrophotometer (Shimadzu, Japan). The SPR experiments were performed using SPR systems integrated with an electrochemical

workstation (Echo Chemie B.V., The Netherlands) based on the Kretschmann optical configuration and using a fixed monochromatic p-polarized laser ($\lambda = 670$ nm) as the light source. Using a vibrating mirror to modulate the angle of incidence of the p-polarized light beam on the SPR substrate, the incidence angle (θ_{SPR}) was obtained by measuring the intensity of reflected light with a photodiode detector over a dynamic range of 4000 m° (4°). A 48-nm-thick gold layer with a 1.5-nm titanium sublayer serving as the adhesive layer were deposited on BK-7 glass and mounted on a hemicylindrical lens using an index-matching oil ($n_d^{25\,°C} = 1.518$). The cuvette in the Autolab SPR instrument contains a standard three-electrode system capable of simultaneous electrochemical measurements. A modified gold chip was used as the working electrode (with an area of 2.5 mm^2 exposed to the solution), a platinum rod was used as the counterelectrode and an Ag/AgCl wire was used as the reference electrode. The surface properties of the modified sensor surface were characterized at each step using electrochemical methods. Voltammograms were recorded in voltage sweeps between −0.05 and 0.6 V with a sweep rate of 50 mV s^{-1} in PBS (pH 7.0). The electrochemical impedance spectroscopy (EIS) measurements were performed in the presence of a 2.5 mM $K_3[Fe(CN)_6]/K_4[Fe(CN)_6]$ (1:1) mixture as a redox probe in PBS containing 0.1 M KCl (pH 7.0) by applying an alternating current voltage with an amplitude of 5 mV over a frequency range of 0.01–10^5 Hz.

2.3. Preparation of ferrocene-branched chitosan derivatives (CS-Fc)

Ferrocene-branched chitosan (CS-Fc) was prepared as described previously with slight modifications [33]. Briefly, CS (75 mg) was dissolved in a 0.1 M acetic acid solution (15 mL). Fc-CHO (20 mg) was dissolved in methanol (15 mL) and then added to the above acidic CS solution. After the mixture was stirred at room temperature for 2 h, $NaCNBH_3$ (100 mg) was added, and the reaction mixture was stirred for another 24 h. The reaction was quenched by precipitation with 5% NaOH, and the yellow product was exhaustively washed with ethanol and water. The product was dried in air and finally redispersed in 0.2 M acetate buffer (pH 5.0) by sonication.

2.4. Synthesis of Fe_3O_4@Au MNPs

The Fe_3O_4 NPs used as seeds were prepared using a previously reported chemical coprecipitation method [34]. In brief, an aqueous solution (180 mL) containing 11.2 mM Fe^{3+} and 5.6 mM Fe^{2+} in a 250 mL flask was heated to 50 °C while removing O_2 by bubbling N_2 into the flask. Next, 12.5 mL of $NH_3{\cdot}H_2O$ was added with vigorous stirring. After 30 min, the precipitate was collected on the vessel wall with a permanent magnet and then washed three times with water. The collected magnetic nanoparticles were diluted to 200 mL with water and treated with ultrasound for 30 min under N_2 protection.

The core–shell Fe_3O_4@Au MNPs were synthesized by growing Au layers on the Fe_3O_4 surface using Wu's method [35]. To modify the surface of the core–shell magnetic nanoparticles with amino groups, 180 μL of APTES was dropped into the Fe_3O_4 suspension (10 mg mL^{-1}, 2 mL) under stirring, and the mixture was agitated for 7 h at room temperature. The APTES-coated Fe_3O_4 NPs were then magnetically separated, washed with ethanol and dispersed in ethanol. Next, 20 mL of APTES-coated Fe_3O_4 NPs (0.5 mg mL^{-1}) and 15 mL of $HAuCl_4$ solution (1% mass fraction) were mixed by sonication, and 20 mM sodium citrate was then dropped into the mixture until the color changed from yellow to black. The resulting dark material was precipitated and separated with a magnetic field and washed with ethanol.

2.5. Preparation of Fe_3O_4@Au MNPs coupled with AFP antibody (Fe_3O_4@Au–Ab_2)

A solution of Ab_2 was added to 5 mL of a Fe_3O_4@Au MNP suspension and stirred for 12 h. After magnetic separation, 50 μL of a 0.25% BSA solution was added to cover the nonspecific sites of the Au layer. After stirring for another 1 h, the Fe_3O_4@Au–Ab_2 composites were precipitated with a magnet and then dispersed in PBS (pH 7.0) and stored at 4 °C when not in use.

2.6. Sensor construction

Scheme 1B is a schematic illustration of the stepwise preparation process of the sensor surface. Initially, to eliminate any possible contamination, the bare gold chip was incubated in Piranha solution (containing sulfuric acid and hydrogen peroxide in a 70%:30%, v:v) for 2 min. After washing with absolute ethanol followed by washing with double-distilled water, the cleaned gold chip was thoroughly dried with N_2 and then placed on the prism with the index-matching oil and covered with the cuvette. Then, 50 μL of a freshly prepared 0.02 M MPS solution (containing 0.01 M H_2SO_4) was injected into the cuvette and held for 2 h to form negatively charged surface. Subsequently, 50 μL of a CS-Fc suspension (2 mg mL^{-1}) was injected into cuvette to assemble a positively charged CS-Fc monolayer. Due to the interactions between the amino (—NH_2) groups of chitosan and the Au NPs, the Au NPs were immobilized on the sensor chip. After a thorough rinsing with PBS (pH 7.0), Ab_1 was injected into the cuvette and then immobilized on the gold sensor surface due to the intense adsorption between the Au NPs and Ab_1. Finally, 50 μL of a 0.25% BSA solution was injected to block any possibly remaining active sites on the nano-Au monolayer. The fabrication of the CS-Fc/Au NP/Ab_1/BSA sensor interface was completed by thoroughly washing the modified sensor chip with PBS.

2.7. Real-time detection of AFP with amplification by Fe_3O_4@Au–Ab_2 conjugates

The amplification of AFP detection was conducted in the form of a sandwich immunoassay using the Fe_3O_4@Au–Ab_2 conjugates for amplification, and adjustments were made by altering the concentration of AFP antigen added to the Fe_3O_4@Au–Ab_2 conjugate solution. The detection procedure consisted of two steps: first, the Fe_3O_4@Au–Ab_2 solution was mixed with various concentrations of AFP antigen to form Fe_3O_4@Au–Ab_2–Ag conjugates, which were then separated and enriched using a magnet, as illustrated in Scheme 1A. Second, the resulting Fe_3O_4@Au–Ab_2–Ag conjugate solution was injected into the SPR cuvette and allowed to react for 30 min, the solution was then drained out with a peristaltic pump, and 50 μL of PBS (pH 7.0) was injected for the dissociation measurements. These processes were performed with a customized, semi-automatic program sequence and monitored in real time with data acquisition software.

3. Results and discussion

3.1. Characteristics of the functionalized nanoparticles

We used a sonochemical method for the synthesis of very high saturation magnetization core–shell Fe_3O_4@Au nanoparticles. TEM images showed that both the Fe_3O_4 and Fe_3O_4@Au NPs were of well spherical structure and high monodispersity in size [36]. The average diameter were about 8–10 nm and 25–30 nm for the purified Fe_3O_4 NPs and the formed core–shell Fe_3O_4@Au NPs, respectively. The thickness of the Au shell was determined to be ~9 nm thick. As reported, the thickness of the shell layer could be changed by

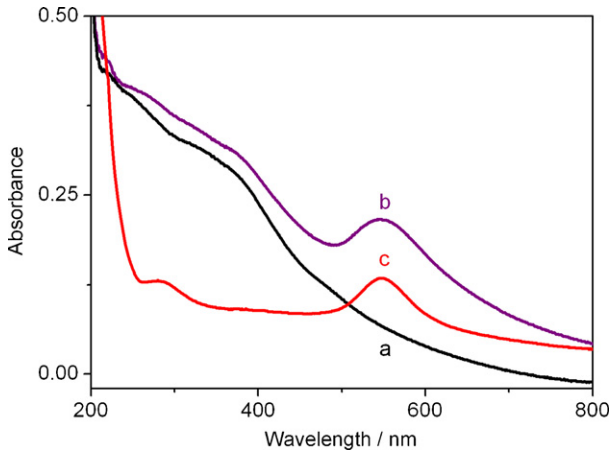

Fig. 1. UV–vis spectra of the Fe_3O_4 MNPs (a), Fe_3O_4@Au MNPs (b), and Fe_3O_4@Au–Ab_2 conjugates (c).

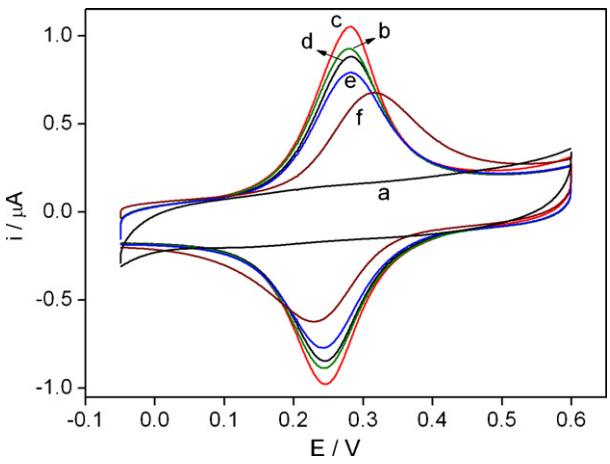

Fig. 2. Cyclic voltammograms of differently modified sensor surfaces in PBS (pH 7.0) at a scan rate of 50 mV s^{-1}. Bare gold chip (a), CS-Fc (b), CS-Fc/Au NPs (c), CS-Fc/Au NPs/Ab_1 (d), CS-Fc/Au NPs/Ab_1/BSA (e) modified chips and an electrode (e) incubated with 100 ng mL^{-1} AFP (f).

varying the experimental parameters [37]. However, proper shell thickness is essential to obtain high enough magnetic-field intensity and stability of the magnetic nanoparticles. Moreover, different size of nanocomposites can impact the SPR response, as the diameter of nanocomposite immobilized in the SPR biosensor increases, the SPR curve can be expected to shift to longer wavelength, which has been proved to be beneficial to enhance the sensitivity of SPR biosensor [38]. While, the parameters of plasmon angle, minimum reflectance, and curve breadth increase with particle diameter, the nanoparticles with too large size will cause a larger reflectance, the SPR curve bears little resemblance to that of a bare evaporated film; the curve is very shallow and broad, without the well defined plasmon angle that is typically observed in SPR [39]. Wang and co-workers compared the SPR angel shift afford by MNPs with different size to understand the size effect of MNPs on the SPR response, it was demonstrated that the MNPs with larger diameter (32.8 nm) have slightly higher affinity for adsorption and much larger angle shifts due to their larger molecular weight [21]. Therefore, the nanocomposites with 25–30 nm are suitable for further experiments.

The formation of Fe_3O_4@Au–Ab_2 conjugates was characterized by UV–vis absorption spectra (Fig. 1). It was evident that the absorbance intensity of the Fe_3O_4 MNPs decreased monotonically with increasing light wavelength in the range of 200–800 nm (Fig. 1a), which is in agreement with results found in the literature [26]. When the Au coating was deposited around the Fe_3O_4 MNPs, a new absorption band centered at 545 nm is clearly observed (Fig. 1b), indicating the formation of $(Fe_3O_4)_{core}$–Au_{shell} MNPs [36]. Upon immobilization of the AFP antibody on the Fe_3O_4@Au MNPs, the characteristic absorption peak of the Fe_3O_4@Au MNPs decreases, and the characteristic adsorption of the AFP antibody clearly appears at 278 nm (Fig. 1c), suggesting the successful immobilization of AFP antibody on the core–shell Fe_3O_4@Au MNP surface.

3.2. Characterization of modified SPR sensor chips with electrochemistry

Fig. 2 presents cyclic voltammograms (CVs) obtained during the stepwise assembly of the SPR biosensor in the potential range of −0.05 to 0.6 V in PBS (pH 7.0) at a scan rate of 50 mV s^{-1}. No redox peaks appear in the CVs of the bare gold film (Fig. 2a) as the lack of redox mediator, whereas the redox hybrid material CS-Fc modified sensor chip displays two well-defined reversible redox peaks for Fc at 281 and 243 mV (Fig. 2b), indicating that Fc was covalently bound in the CS chain and that a CS-Fc complex was assembled on the sensor surface by electrostatic adsorption. The further deposition of Au NPs increased the conductivity of the CS-Fc film, resulting in increases in the anodic peak and cathodic peak currents (Fig. 2c) because Au NPs act as a conducting wire or an electron communication relay, which increases the electron-transfer efficiency of the surface [40–42]. When the CS-Fc/Au NP film was incubated with the primary AFP antibody, the redox peak currents decreased significantly (Fig. 2d), which, on one hand, indicates that the antibody had been successfully immobilized on the CS-Fc/Au NPs film surface and, on the other hand, that the immobilized protein acts as an insulator, blocking electron communication between the Fc and the electrode. When BSA was employed to block any possibly remaining active sites on the nano-Au monolayer, the redox peak currents decreased further (Fig. 2e). Interestingly, after AFP antigen molecules specifically recognized the immobilized AFP antibody, the redox peak currents of the Fc clearly decreased, and the peak-to-peak separation increased (Fig. 2f), again indicating that the formation of the immunocomplex further hinders the electron-transfer pathway of the covalently bound Fc [43,44].

EIS is a sensitive and powerful characterization tool that can provide detailed information on changes in the surface properties of modified electrodes in a stepwise modification process. The typical impedance spectrum (presented in the form of a Nyquist plot) includes a semicircle portion at higher frequencies corresponding to the electron-transfer-limited process and a linear part at lower frequency range representing the diffusion-limited process. The semicircle diameter in the impedance spectrum is equal to the electron-transfer resistance (R_{et}), which reflects the electron-transfer kinetics of the redox probe at the electrode surface. Fig. 3 presents the impedance spectra corresponding to each modification process in the presence of the redox probe $Fe(CN)_6^{3-/4-}$ measured at the formal potential. The bare gold chip exhibits an almost straight line (Fig. 3a), indicating a diffusion-limited electron-transfer process. After the immobilization of a CS-Fc layer, the value of R_{et} increased to 1707 Ω (Fig. 3b), which indicated the successful formation of a CS-Fc membrane, thus partly blocking the electron transfer of $[Fe(CN)_6]^{3-/4-}$ solution to the electrode [45]. When Au NPs were assembled, the R_{et} of the resulting CS-Fc/Au NPs film surprisingly decreased to 1035 Ω (Fig. 3c), indicating that the excellent electric conductivity of the Au NPs accelerates electron transfer between the electrochemical probe and the electrode. When Ab_1 molecules were bound to the CS-Fc/Au NPs film, the R_{et} increased to 2445 Ω (Fig. 3d); after the AFP antigen molecules were coupled onto the CS-Fc/Au NP/Ab_1-modified electrode, a remarkable increase of the interfacial resistance to 3712 Ω was obtained

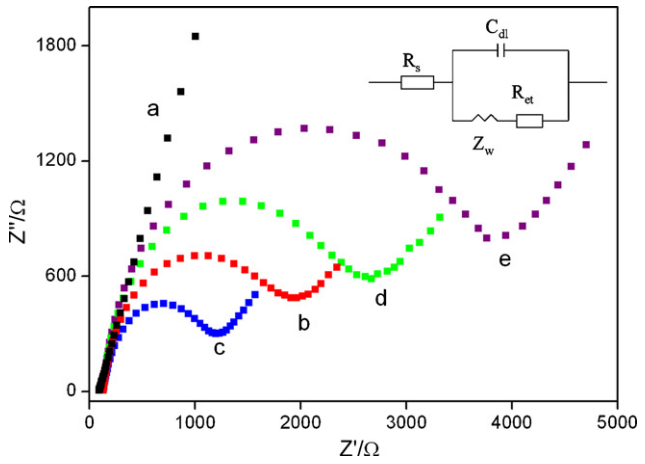

Fig. 3. Nyquist plots of the different SPR sensor surfaces in a PBS solution (0.1 M, pH 7.0) containing 0.1 M KCl and 2.5 mM $Fe(CN)_6^{3-/4-}$: bare gold chip (a), CS-Fc (b), CS-Fc/Au NPs (c), CS-Fc/Au NPs/Ab_1 (d), and CS-Fc/Au NPs/Ab_1/Ag (e). The inset is the equivalent circuit used to model the impedance data in the presence of the redox couple. R_s, Z_w, R_{et} and C_{dl} represent the solution resistance, the Warburg diffusion resistance, the electron-transfer resistance, and the double-layer capacitance, respectively.

(Fig. 3e). The reason for this dramatic increase is that the immunocomplex layer on the electrode blocks electron communication and mass transfer, further insulating the conductive support and significantly hindering the access of the redox probe to the electrode surface; thus, a further increase in R_{et} is observed [40,46,47]. The EIS changes during the modification process indicate that the Ab_1 was firmly immobilized on the CS-Fc/Au NPs film electrode surface and retained high bioactivity, which is in good agreement with the CV results.

3.3. Magnetic nanoparticles amplify the SPR signal

Three separate AFP detection protocols demonstrated the level of amplification provided by the Fe_3O_4@Au MNPs. Fig. 4A illustrates the three protocols for the detection of AFP and the amplification of the detection signal: (a) the direct detection of free AFP in PBS, (b) amplification with Ab_2, and (c) amplification with Fe_3O_4@Au–Ab_2 conjugates. Fig. 4B shows a schematic diagram of the three protocols and the relative size of each particle. In the direct detection format (a), a small SPR angle shift of $\Delta\theta_a = 20\,m^\circ$ was observed, as seen in curve a in Fig. 4A. The SPR angle shift ($\Delta\theta_b = 102\,m^\circ$) resulting from the binding of Ab_2–Ag (Fig. 4A, curve b) is approximately 5-fold higher than that resulting from the direct adsorption of biomolecules. It should be noted that the SPR angle shift greatly increased, to 328 m°, when the Fe_3O_4@Au–Ab_2 conjugates were used (Fig. 4A, curve c), a value approximately 16.4 times higher than that for the direct detection format at the same antigen concentration, further demonstrating the dramatic amplification of Fe_3O_4@Au MNPs in the SPR sensing protocol. The reason can be attributed to the three aspects: first, the high surface-to-volume ratio of the core–shell Fe_3O_4@Au MNPs may greatly enhance the immobilization density of bound AFP antibody molecules, and the good biocompatibility of Au shell should maintain the biological activity of the immobilized proteins. Second, the high refractive index and the high molecular weight of the Fe_3O_4 MNPs favor the amplification of the SPR signal [21]. Third, the electronic coupling interaction between the Au shell and the surface plasmon wave associated with the SPR gold film may also result in a significant amplification of the SPR signal [7]. In addition to amplifying the SPR signal, the magnetic properties of the Fe_3O_4@Au MNPs can also be exploited to separate the analyte from the sample matrix (analyte affinity purification) and concentrate the sample prior to introduction to the sensor system. When placed in an external magnetic field, the Fe_3O_4@Au–Ab_2 conjugates can be magnetically separated from the sample solution (Scheme 1A). Removal of the magnet from the column allows the Fe_3O_4@Au–Ab_2 conjugates to be eluted into a smaller volume of buffer prior to injection into the sensor system. The separation/concentration/amplification protocol facilitates the rapid purification of analyte from complex matrixes, allowing for significant amplification of the detection signal compared with the direct detection assay.

3.4. SPR determination of AFP using Fe_3O_4@Au MNPs for signal enhancement

The basis of a particle-enhanced bioassay is that biomolecular interaction events lead to particle immobilization, i.e., more immobilized proteins yield higher particle coverage [48]. After separation and enrichment with a magnet, Fe_3O_4@Au–Ab_2–Ag immunocomplexes with various AFP concentrations were injected into the SPR cuvette; the analysis of different concentrations of AFP using the procedure outlined in Scheme 1A is illustrated in Fig. 5. The verification of analyte identity was achieved simultaneously because antibodies to one analyte epitope were used on the Fe_3O_4@Au MNPs (murine monoclonal anti-AFP) and antibodies to multiple analyte epitopes were immobilized on the sensor surface (mouse polyclonal anti-AFP). The SPR angle shifts resulting from the binding of Fe_3O_4@Au–Ab_2 conjugates gradually increased with increasing AFP antigen concentrations. On analyzing the changes in the SPR angle shift with respect

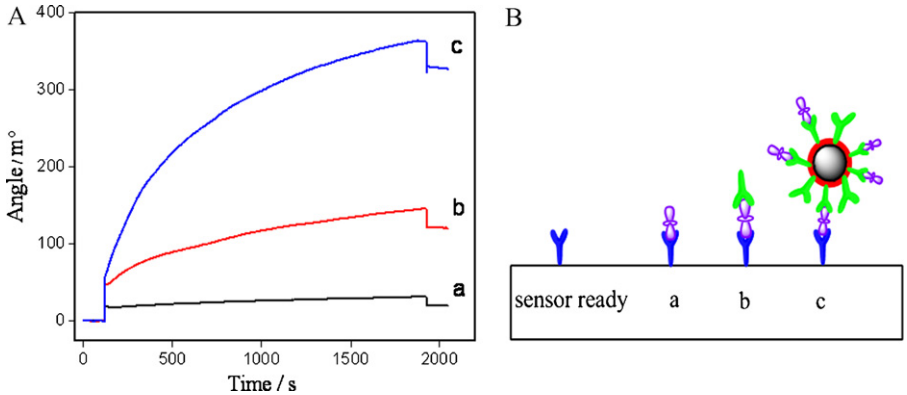

Fig. 4. (A) The SPR response curve for detection of 150 ng mL^{-1} AFP: direct detection of free AFP in PBS (a), amplification with α-fetoprotein antibody (Ab_2) (b), and amplification with Fe_3O_4@Au–Ab_2 conjugates (c). (B) Illustration of the sensor surface, showing the binding and amplified detection.

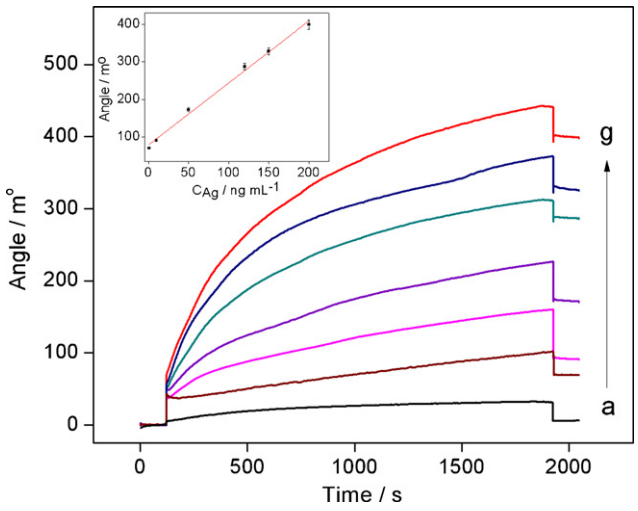

Fig. 5. SPR angle-time curves of the separation products obtained after Fe_3O_4@Au–Ab_2 conjugates were reacted with various concentrations of AFP: blank solution (a); curves (b–g) represent, respectively, 1.0, 10.0, 50.0, 120.0, 150.0, and 200.0 ng mL^{-1}. (Inset) The linear relationship between the AFP concentrations and the SPR angle shifts resulting from the binding of the Fe_3O_4@Au–Ab_2 conjugates.

to the concentration of AFP antigens, a good linear relationship was obtained in the range of 1.0–200.0 ng mL^{-1} (inset in Fig. 5); the linear regression equation for these data is as follows: angle (m°) = 77.25 + 1.66C_{Ag} (R^2 = 0.996). By fitting the binding curves in Fig. 5 with 1:1 binding model, the association constants (k_a) was found to be 4.5×10^5 (M s)$^{-1}$, and the dissociation constants (k_d) to be 1.8×10^{-3} s^{-1}, thus the affinity constants (K_A) was estimated to be 2.5×10^8 M^{-1}, which is somewhat smaller than those of 2.8×10^8 M^{-1} for the detection format (a) and 2.6×10^8 M^{-1} for the detection format (b). The reason is the steric hindrance may affect the affinity for the Fe_3O_4@Au–Ab_2–Ag conjugates with Ab_1 immobilized on the SPR sensor chip. The detection limit is 0.65 ng mL^{-1} at the signal-to-noise ratio of 3, which is lower than those reported 1.6 ng mL^{-1} for a poly(vinyl chloride)/o-phenylenediamine/Au/anti-AFP-based potentiometric biosensor [49], 0.8 μg L^{-1} for a gelatin/Ag/anti-AFP-based potentiometric immunosensor [50], and 2.4 ng mL^{-1} for an anti-AFP/nano-Au/Thi/Nf-based amperometric immunosensor [46]. The lower detection limit and enhanced sensitivity of the newly developed sensor demonstrate that SPR technology is a powerful tool that offers real-time monitoring, label-free detection, and high-specificity binding for characterizing and quantifying biomolecular interactions, and the core–shell Fe_3O_4@Au MNPs are a perfect amplifier for the quantitative determination of AFP concentrations in complex samples.

4. Conclusions

A novel SPR sensor for the detection of AFP with low interference and high sensitivity was constructed based on an MPS/CS-Fc/Au NPs/Ab_1/BSA film using Fe_3O_4@Au–Ab_2 magnetic conjugates as an amplification regent. The core–shell Fe_3O_4@Au MNPs not only have magnetic Fe_3O_4 cores allowing for their easy manipulated in an external magnetic field but also have excellent biocompatibility due to the Au shell, which maintains the bioactivity of immobilized proteins. Moreover, the high refractive index and the high molecular weight of the Fe_3O_4@Au MNPs facilitate the amplification of the SPR signal. The experimental results demonstrate that the designed SPR sensor possesses a good sensitivity and a high selectivity for AFP detection. Importantly, it is simple to generalize this strategy for the detection of a large variety of biomolecules of interest by changing the type of biomolecule used to label the MNPs.

Acknowledgements

This work was supported by grants from the National Natural Science Foundation of China (20805023, 21065006, 21163014), the Program for New Century Excellent Talents in University (NCET-11-1002), and the Program for Young Scientists of Jiangxi Province (20112BCB23001).

References

[1] B. Liedberg, C. Nylander, I. Lundstrom, Sens. Actuators 4 (1983) 299–304.
[2] K.V. Gobi, H. Iwasaka, N. Miura, Biosens. Bioelectron. 22 (2007) 1382–1389.
[3] E. Mauriz, A. Calle, J.J. Manclus, A. Montoya, L.m. Lechuga, Anal. Bioanal. Chem. 387 (2007) 1449–1458.
[4] V. Nanduri, A.K. Bhunia, S.I. Tu, G.C. Paoli, J.D. Brewster, Biosens. Bioelectron. 23 (2007) 248–252.
[5] S.R. Raz, M.G.E.G. Bremer, W. Haasnoot, W. Norde, Anal. Chem. 81 (2009) 7743–7749.
[6] A. Larsson, J. Angbrant, J. Ekeroth, P. Mansson, B. Liedberg, Sens. Actuators B 113 (2006) 730–748.
[7] M. Frasconi, C. Tortolini, F. Botre, F. Mazzei, Anal. Chem. 82 (2010) 7335–7342.
[8] L.Y. Wang, Y. Sun, J. Wang, X.N. Zhu, F. Jia, Y.B. Cao, X.H. Wang, H.Q. Zhang, D.Q. Song, Talanta 78 (2009) 265–269.
[9] P.E. Buckle, R.J. Davies, T. Kinning, D. Yeung, P.R. Edwards, D. Pollard-Knight, C.R. Lowe, Biosens. Bioelectron. 8 (1993) 355–363.
[10] J. Dostalek, J. Homola, Sens. Actuators B 129 (2008) 303–310.
[11] A. Zybin, D. Boecker, V.M. Mirsky, K. Niemax, Anal. Chem. 79 (2007) 4233–4236.
[12] A.N. Naimushin, S.D. Soelberg, D.K. Nguyen, L. Dunlap, D. Bartholomew, J. Elkind, J. Melendez, C.E. Furlong, Biosens. Bioelectron. 17 (2002) 573–584.
[13] Y. Liu, Y. Dong, J. Jauw, M.J. Linman, Q. Cheng, Anal. Chem. 82 (2010) 3679–3685.
[14] K.Q. Lin, Y.H. Lu, J.X. Chen, R.S. Zheng, P. Wang, H. Ming, Opt. Express 16 (2008) 18599–18604.
[15] J.L. Wang, H.S. Zhou, Anal. Chem. 80 (2008) 7174–7178.
[16] X. Huang, H.Y. Tu, D.H. Zhu, D. Du, A.D. Zhang, Talanta 78 (2009) 1036–1042.
[17] J. Yuan, R. Oliver, M.I. Aguilar, Y.Q. Wu, Anal. Chem. 80 (2008) 8329–8333.
[18] S. Ko, T.J. Park, H.S. Kim, J.H. Kim, Y.J. Cho, Biosens. Bioelectron. 24 (2009) 2592–2597.
[19] D. Beccati, K.M. Halkes, G.D. Batema, G. Guillena, A.C. de Souza, G.V. Koten, J.P. Kamerling, ChemBioChem 6 (2005) 1196–1203.
[20] L.A. Lyon, M.D. Musick, M.J. Natan, Anal. Chem. 70 (1998) 5177–5183.
[21] J.L. Wang, A. Munir, Z.Z. Zhu, H.S. Zhou, Anal. Chem. 82 (2010) 6782–6789.
[22] H.Y. Park, M.J. Schadt, L.Y. Wang, I-I.S. Lim, P.N. Njoki, S.H. Kim, M.-Y. Jiang, J. Luo, C.J. Zhong, Langmuir 23 (2007) 9050–9056.
[23] X.L. Zhao, Y.Q. Cai, T. Wang, Y.L. Shi, G.B. Jang, Anal. Chem. 80 (2008) 9091–9096.
[24] Z.C. Xu, Y.L. Hou, S.H. Sun, J. Am. Chem. Soc. 129 (2007) 8698–8699.
[25] S.J. Cho, J.C. Idrobo, J. Olamit, K. Liu, N.D. Browning, S.M. Kauzlarich, Chem. Mater. 17 (2005) 3181–3186.
[26] D.P. Tang, R. Yuan, Y.Q. Chai, J. Phys. Chem. B 110 (2006) 11640–11646.
[27] Y.H. Deng, D.W. Qi, C.H. Deng, X.M. Zhang, D.Y. Zhao, J. Am. Chem. Soc. 130 (2008) 28–29.
[28] J.D. Qiu, H.P. Peng, R.P. Liang, Electrochem. Commun. 9 (2007) 2734–2738.
[29] C.T. Chen, Y.C. Chen, Anal. Chem. 77 (2005) 5912–5919.
[30] Y. Li, Y.C. Liu, J. Tang, H.Q. Lin, N. Yao, X.Z. Shen, C.H. Deng, P.Y. Yang, X.M. Zhang, J. Chromatogr. A 1172 (2007) 57–71.
[31] Y.R. Yuan, R. Yuan, Y.Q. Chai, Y. Zhuo, Y.T. Shi, H.L. He, X.M. Miao, Electroanalysis 19 (2007) 1402–1410.
[32] E. Hutter, J.H. Fendler, D. Roy, J. Phys. Chem. B 105 (2001) 11159–11168.
[33] W.W. Yang, H. Zhou, C.Q. Sun, Macromol. Rapid Commun. 28 (2007) 265–270.
[34] C.Q. Yang, G. Wang, Z.Y. Lu, J. Sun, J.Q. Zhuang, W.S. Yang, J. Mater. Chem. 15 (2005) 4252–4257.
[35] W. Wu, Q.G. He, H. Chen, J.X. Tang, L. Nie, Nanotechnology 18 (2007) 145606–145609.
[36] J.D. Qiu, H.P. Peng, R.P. Liang, X.H. Xia, Biosens. Bioelectron. 25 (2010) 1447–1453.
[37] L.Y. Wang, J. Luo, Q. Fan, M. Suzuki, I.S. Suzuki, M.H. Engelhard, Y.H. Lin, N. Kim, J.Q. Wang, C.J. Zhong, J. Phys. Chem. B 109 (2005) 21593–21601.
[38] J. Homola, Sens. Actuators B 41 (1997) 207–211.
[39] L.A. Lyon, D.J. Pen, M.J. Natan, J. Phys. Chem. B 103 (1999) 5826–5831.
[40] J.D. Qiu, R.P. Liang, R. Wang, L.X. Fan, Y.W. Chen, X.H. Xia, Biosens. Bioelectron. 25 (2009) 852–857.
[41] J.D. Qiu, R. Wang, R.P. Liang, X.H. Xia, Biosens. Bioelectron. 24 (2009) 2920–2925.
[42] J. Chen, F. Yan, D. Du, J. Wu, H.X. Ju, Electroanalysis 18 (2006) 670–676.
[43] N. Li, R. Yuan, Y.Q. Chai, S.H. Chen, H.Z. An, W.J. Li, J. Phys. Chem. C 111 (2007) 8443–8450.

[44] Y. Wu, J. Zheng, Z. Li, Y. Zhao, Y. Zhang, Biosens. Bioelectron. 24 (2009) 1389–1393.
[45] Z.L. Wei, Z.J. Li, X.L. Sun, Y.J. Fang, J.K. Liu, Biosens. Bioelectron. 25 (2010) 1434–1438.
[46] Y. Zhuo, R. Yuan, Y.Q. Chai, D.P. Tang, Y. Zhang, N. Wang, X.L. Li, Q. Zhu, Electrochem. Commun. 7 (2005) 355–360.
[47] Y. Zhuo, P.X. Yuan, R. Yuan, Y.Q. Chai, C.L. Hong, Biomaterials 29 (2008) 1501–1508.
[48] L.A. Lyon, D.J. Pena, M.J. Nantan, J. Phys. Chem. B 103 (1999) 5826–5831.
[49] L. Zhou, R. Yuan, Y.Q. Chai, Electroanalysis 19 (2007) 1131–1138.
[50] Z. Qiang, R. Yuan, Y.Q. Chai, N. Wang, Y. Zhuo, Y. Zhang, X.L. Li, Electrochim. Acta 51 (2006) 3763–3768.